Supplementary Information

Detection of a few DNA copies by real-time electrochemical polymerase chain reaction

M. Moreau,[a] S. Delile,[a] A. Sharma,[a,b] C. Fave,[a] A. Perrier,* [b,c] B. Limoges,* [a] and D. Marchal* [a]

[a] *Laboratoire d'Electrochimie Moléculaire, UMR 7591 CNRS, Université Paris Diderot, Sorbonne Paris Cité, 15 rue Jean-Antoine de Baïf, F-75205 Paris Cedex 13, France.*

[b] *Equipe de Chimie Théorique et Modélisation (CTM), Chimie ParisTech, PSL Research University, CNRS, Institut de Recherche de Chimie Paris (IRCP), F-75005 Paris, France.*

[c] *Université Paris Diderot, Sorbonne Paris Cité, 5 rue Thomas Mann, F-75205 Paris Cedex 13, France.*

Table of Contents

1. Illustrative examples of the SWV responses and resulting raw kinetic PCR plots obtained for each redox probe during the PCR amplification of a positive sample

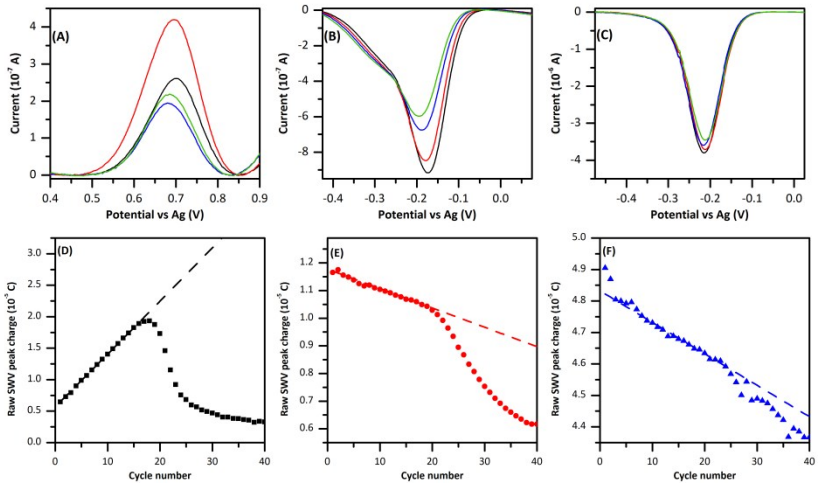

Fig. S1 Top: baseline-corrected SWV responses measured during the qPCR amplification of 10^7 DNA copies of litmus 28i vector in the presence of (A) 0.5 µM $[Os(bpy)_2dppz]^{2+}$, (B) 15 µM PhP and (C) 15 µM MB. The SWV responses were recorded at the PCR cycle number: (black) 10, (red) 20, (blue) 30 and (green) 40. Bottom: raw electrochemical qPCR curves (i.e., before baseline correction and normalisation) obtained in the presence of (D) 0.5 µM $[Os(bpy)_2dppz]^{2+}$, (E) 15 µM PhP and (F) 15 µM MB.

2. Electrochemical determination of K_b as a function of temperature for each of the redox probes

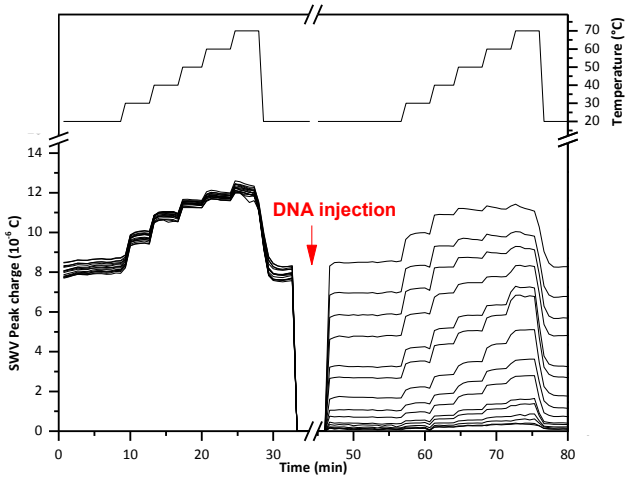

Fig. S2 Experimental determination of the binding constant of $[Os(bpy)_2dppz]^{2+}$ (C_I^0 = 20 µM) to calf-thymus DNA at different temperatures. Top: profile of the staircase ramp of temperature applied as a function of time to the overall solutions deposited in a 48-well electrochemical microplate (here 15 triplicated solutions of 40 µL monitored electrochemically in parallel). Bottom: evolution of the SWV peak charge as a function of time (one measurement every 40 s). A series of different standard concentrations of calf-thymus DNA (i.e., serially diluted in such a way to range from C_{DNA}^0 = 0 to 2.5 × 10^{-4} M^{-1}) was injected into the electrochemical wells at the time interval of 35-45 min (red arrow).

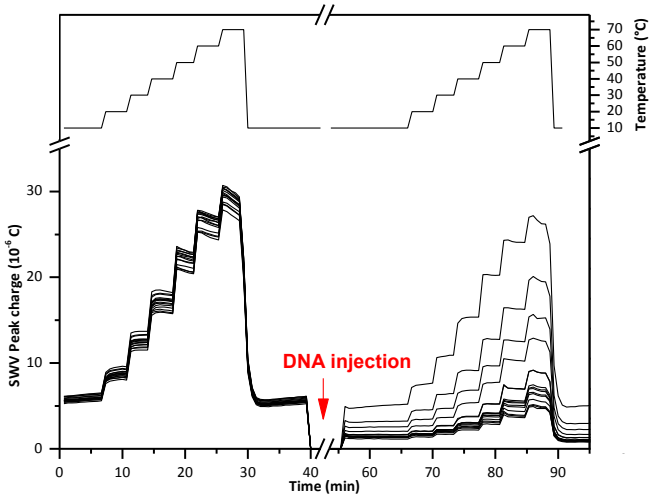

Fig. S3 Experimental determination of the binding constant of PhP (C_I^0 = 20 µM) to calf-thymus DNA at different temperatures. Top: profile of the staircase ramp of temperature applied as a function of time to the overall solutions deposited in a 48-well electrochemical microplate (here 15 triplicated solutions of 40 µL monitored electrochemically in parallel). Bottom: evolution of the SWV peak charge as a function of time (one measurement every 40 s). A series of different standard concentrations of calf-thymus DNA (i.e., serially diluted in such a way to range from C_{DNA}^0 = 0 to 4.0 × 10^{-4} M^{-1}) was injected into the electrochemical wells at the time interval of 42-55 min (red arrow).

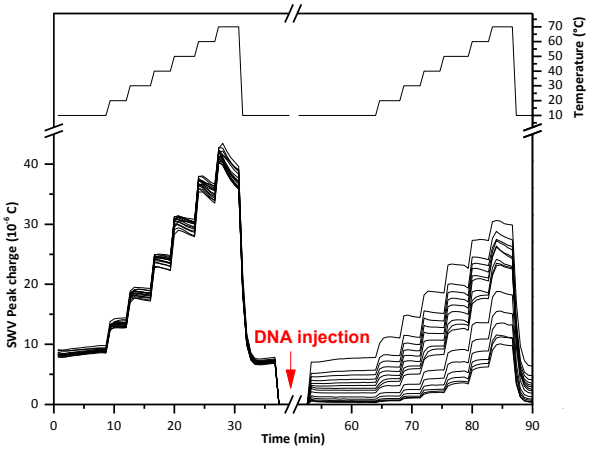

Fig. S4 Experimental determination of the binding constant of MB (C_I^0 = 20 µM) to calf-thymus DNA at different temperatures. Top: profile of the staircase ramp of temperature applied as a function of time to the overall solutions deposited in a 48-well electrochemical microplate (here 15 triplicated solutions of 40 µL monitored electrochemically in parallel). Bottom: evolution of the SWV peak charge as a function of time (one measurement every 40 s). A series of different standard concentrations of calf-thymus DNA (i.e., serially diluted in such a way to range from C_{DNA}^0 = 0 to 7.65 × 10^{-4} M^{-1}) was injected into the electrochemical wells at the time interval of 40-55 min (red arrow).

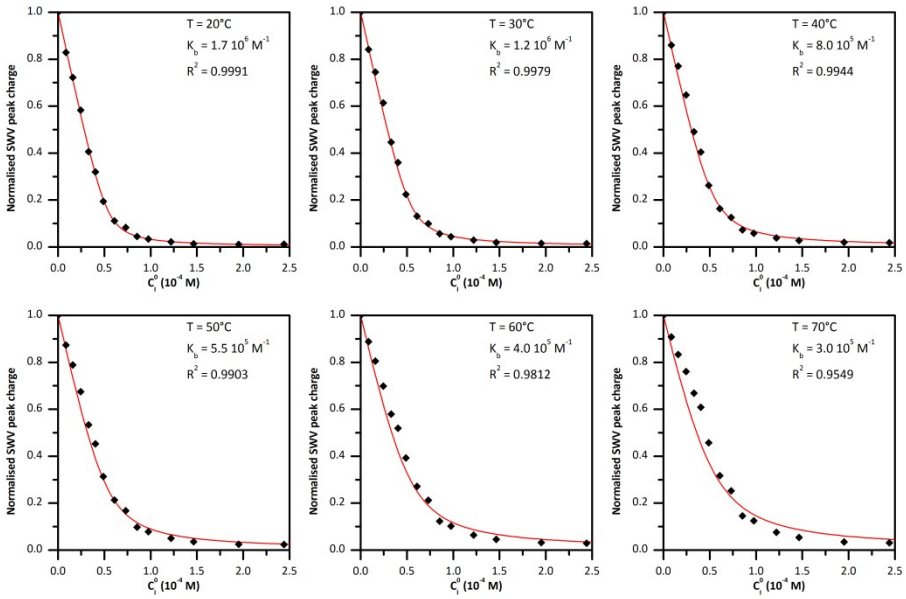

Fig. S5 Normalised SWV peak charge as a function of the total base pair concentration C_{DNA}^0 for $[Os(bpy)_2dppz]^{2+}$ binding experiment at 20, 30, 40, 50, 60 and 70°C (data extracted from Fig. S2). Black diamonds: experimental data (average of triplicates). Red line: best fit using eq S1 (K_b and correlation coefficient R^2 are indicated on each figure, *s* is 2.8 bp).

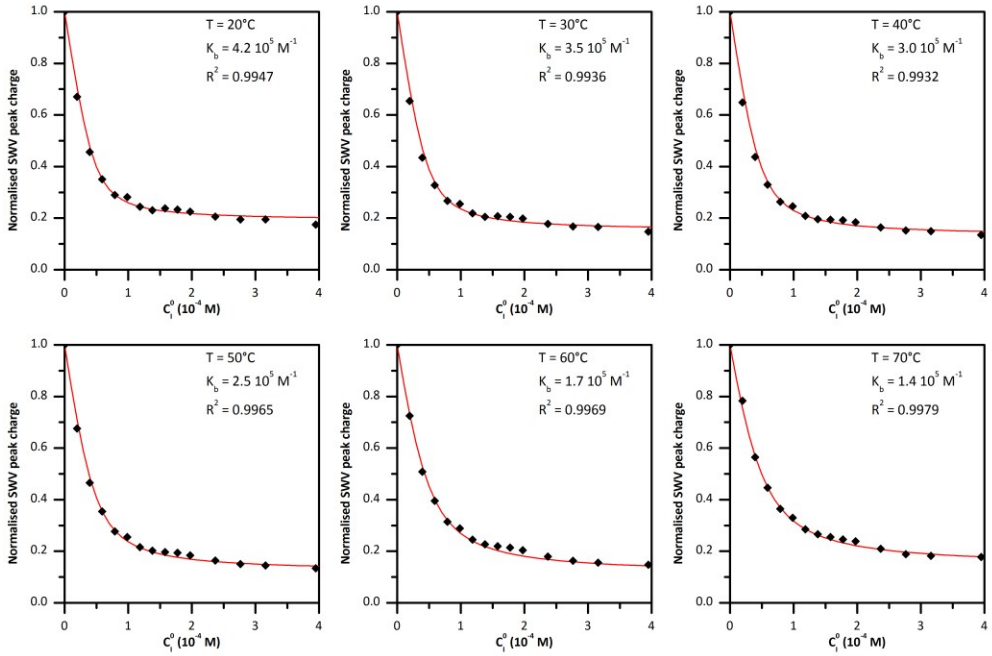

Fig. S6 Normalised SWV peak charge as a function of the total base pair concentration C^0_{DNA} for PhP binding experiment at 20, 30, 40, 50, 60 and 70°C (data extracted from Fig. S3). Black diamonds: experimental data (average of triplicates). Red line: best fit using eq S1 (K_b and correlation coefficient R^2 are indicated on each figure, *s* is 2.3 bp).

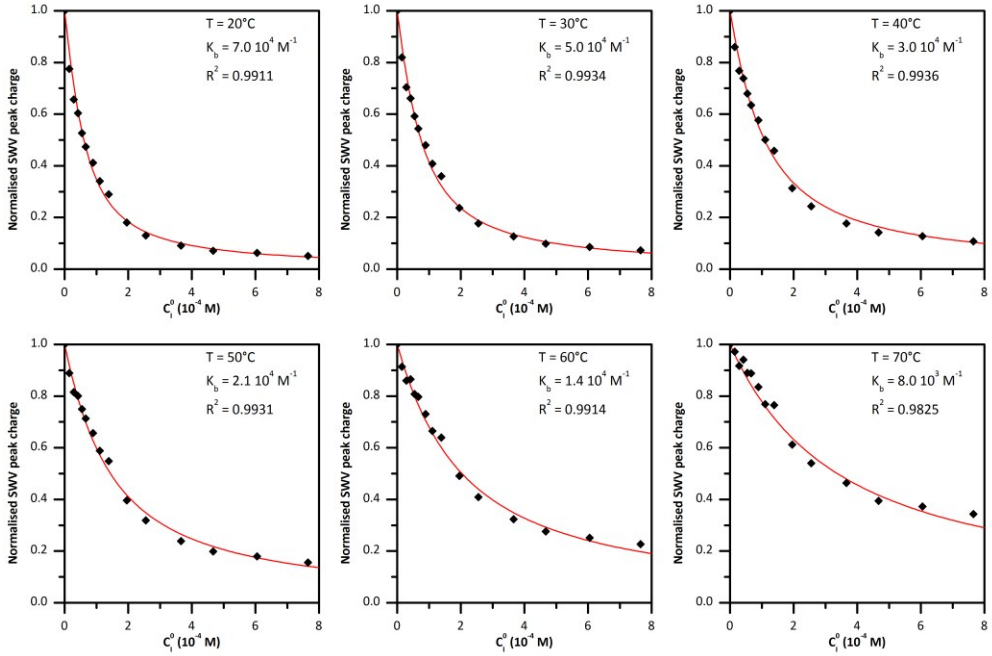

Fig. S7 Normalised SWV peak charge as a function of the total base pair concentration C^0_{DNA} for MB binding experiment at 20, 30, 40, 50, 60 and 70°C (data extracted from Fig. S4). Black diamonds: experimental data (average of triplicates). Red line: best fit using Eq S1 (K_b and correlation coefficient R^2 are indicated on each figure, *s* is 2.5 bp).

3. Molecular Dynamics Study of DNA-probe complex

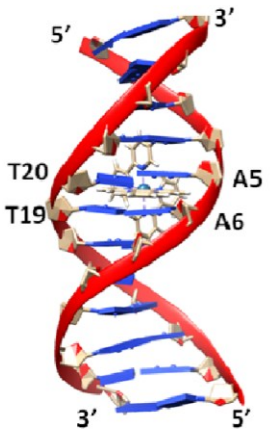

Int-Major

Fig. S8 Initial structure of the $[Os(bpy)_2dppz]^{2+}$ complex in interaction with the long axis of 1BNA. intercalation in the major groove (Int-Major).

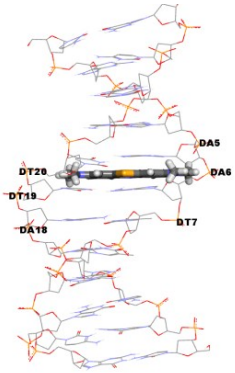

MB

symmetrical intercalation

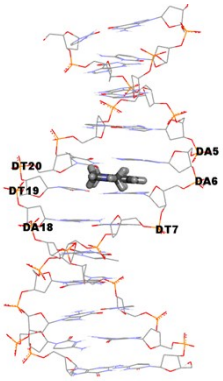

MB

perpendicular intercalation

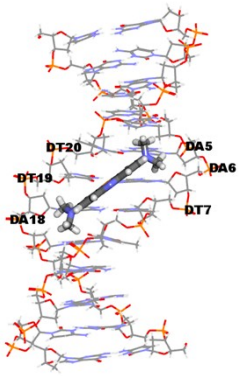

MB

minor groove binding

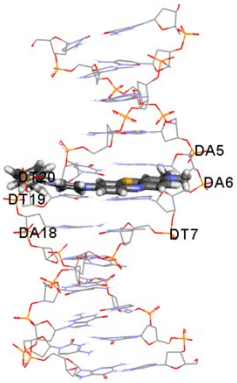

PhP

symmetrical intercalation

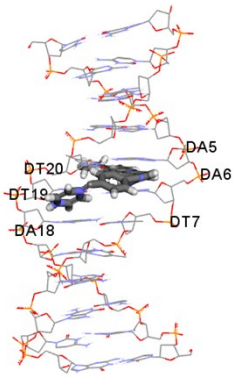

PhP

perpendicular intercalation

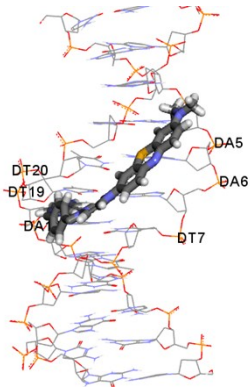

PhP

minor groove binding

Fig. S9 Initial structures of MB and PhP probe molecules in interaction with the long axis of 1BNA

[Os(bpy)$_2$dppz]$^{2+}$. At 25°C, the major groove intercalation is a stable binding mode and as shown in our previous studies,[S1] this stability arises from π-π interactions. This intercalation mode remains stable when the temperature increases (Figs. S10a and S10b). However, the Root-Mean-Square Deviation (RMSD) of the 1BNA in Fig. S10c shows strong structural distortions of the DNA which leads to less effective π-π stacking. This leads to a lessening of the interaction between the probe and the dsDNA as experimentally shown.

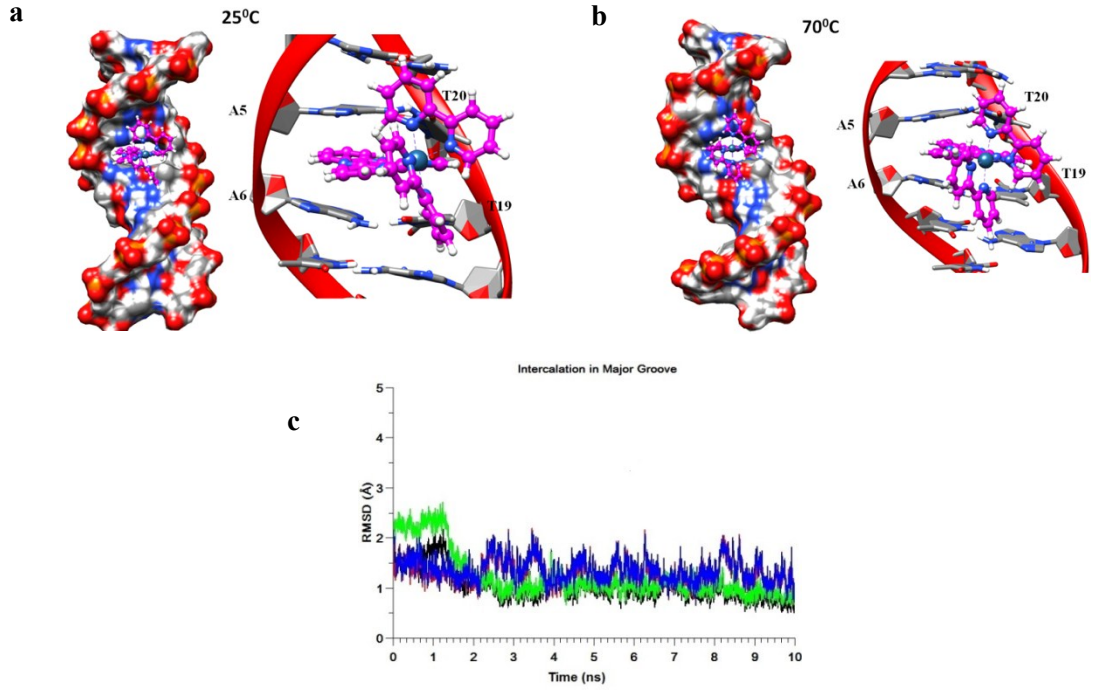

Fig. S10 Snapshots of the [Os(bpy)$_2$dppz]$^{2+}$ probe intercalation in the major groove of 1BNA at (a) 25^{0}C and (b) 70^{0}C. (c) plot of the RMSD obtained for the DNA:1BNA, at 25^{0}C, Avg RMSD=1.04(0.3)Å (black) and 70^{0}C, Avg RMSD=1.31(0.3)Å (red). For the [Os(bpy)$_2$dppz]$^{2+}$/1BNA complex at 25^{0}C, Avg RMSD=1.22(0.5)Å (green) and 70^{0}C, Avg RMSD=1.36(0.3)Å (blue). Average values of the RSMD with their standard deviation are also given.

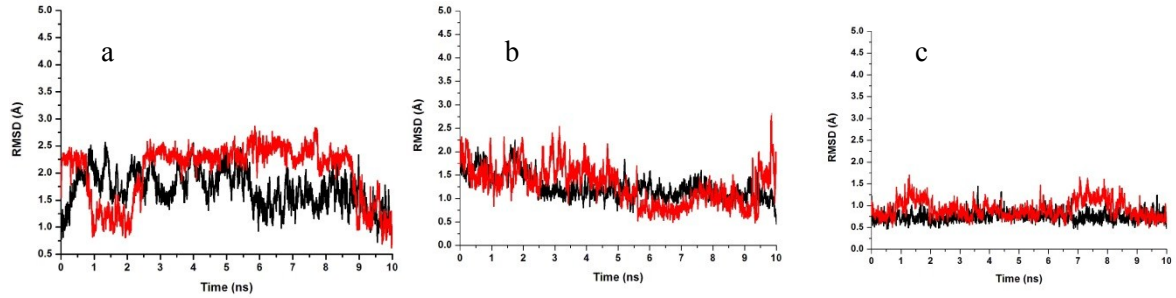

Fig. S11 Plot of the RMSD obtained for the MB / 1BNA complex for the three binding modes (a) Symmetrical intercalation at 25^{0}C, Avg RMSD=1.71(0.3)Å (black) and 70^{0}C, Avg RMSD=2.03(0.5)Å (red), (b) perpendicular intercalation at 25^{0}C, Avg RMSD=1.24(0.3)Å (black) and 70^{0}C, Avg RMSD=1.30(0.4)Å (red), and (c) minor groove binding at 25^{0}C, Avg RMSD=0.75 (0.1)Å (black) and 70^{0}C, Avg RMSD=0.92 (0.2)Å (red).

MB. (*i*) At 25°C, the perpendicular and symmetrical intercalation binding modes are stable due to the formation of π-π interactions. On Figs. S11a and S11c, the RMSD shows a strong distortion of the DNA intercalation pocket as the temperature increases. These yield to less effective π-π stacking and thus to a destabilisation of these intercalation modes. This temperature effect on the intercalation pocket of DNA has been also shown by the intercalation binding mode of the $[Os(bpy)_2dppz]^{2+}$/1BNA complex. Therefore, it predicts that like $[Os(bpy)_2dppz]^{2+}$, the intercalation of the MB decreases with increasing in the temperature. Moreover one can note that for MB, there is less RMSD fluctuation for perpendicular intercalation than symmetrical intercalation, however the average value of RMSD for $[Os(bpy)_2dppz]^{2+}$ and MB for perpendicular intercalation mode of binding are indeed closer (Fig. S12). (*ii*) Unlikely $[Os(bpy)_2dppz]^{2+}$, there is another stable binding mode for the MB with the DNA, which corresponds to minor groove binding. This mode arises from the formation of H bonds between the N-H group of a Thymine base and the Sulphur atom of the MB probe. For this mode, there is a small variation of the number of H bonds with the increase of the temperature (Fig. S13). This is due to the flexibility of this binding mode which allows the probe to adapt quasi instantaneously to the DNA deformation. The H bond interactions are thus preserved (Fig. S13). However, for MB, this mode is less stable than intercalation ones as shown by Nogueira and coll.[S2] Please note that in case of minor groove binding there is no intercalation bubble formation in DNA and it is difficult to compare the RMSD with the perpendicular intercalation mode.[S2]

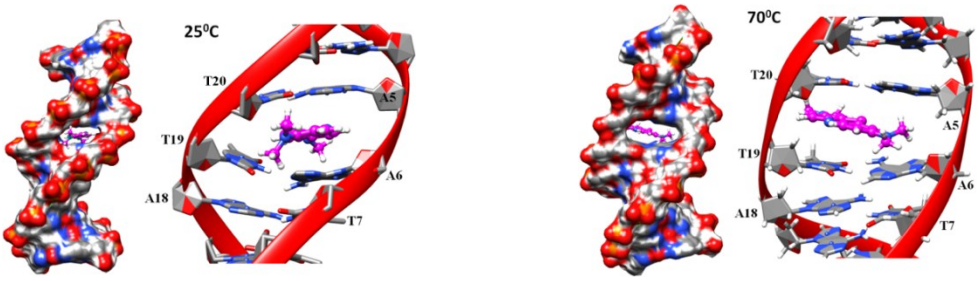

Fig. S12 Snapshots of Methylene Blue (MB) most stable binding mode: perpendicular intercalation in the minor groove at T = 25°C and 70°C.

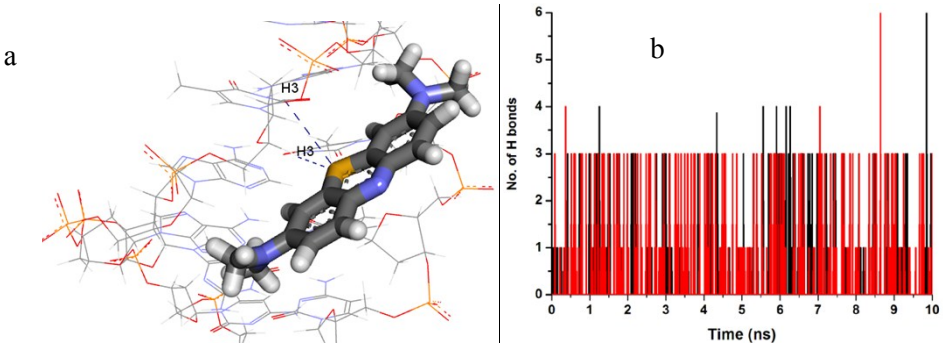

Fig. S13 (a) Snapshot showing the formation of H bonds between 1BNA and MB. (b) Number of H bonds between 1BNA and MB as a function of time along the 10 ns trajectory (for T = 25°C and 70°C). The total number of H bonds formed at T = 25°C are 302 (black) and at 70°C are 401 (red) along the 10 ns trajectory.

PhP. (*i*) At 25°C, intercalation binding modes are stable thanks to the formation of π-π interactions. The RMSD shows a strong distortion of the DNA intercalation pocket as the temperature increases (Figs. S14a and S14c). This yields to less effective π-π stacking and thus to a destabilization of these intercalation modes. These behaviours are thus the same as $[Os(bpy)_2dppz]^{2+}$ and MB. However, in the case of PhP, the perpendicular intercalation mode of binding undergoes higher degree of fluctuation than perpendicular intercalation of $[Os(bpy)_2dppz]^{2+}$ and MB, i.e. higher RMSD value in case of PhP. Therefore, contrary to $[Os(bpy)_2dppz]^{2+}$ and MB, this is not the most stable binding mode in case of PhP. (*ii*) For PhP, like MB, there is another binding mode which corresponds to minor groove binding. This mode arises from the formation of H bonds between DNA base Thymine-N-H....S-PhP, base Adenine-N....HN-PhP and Ribose-O....HN-PhP and base Thymine-O...HN-PhP. Therefore, in the case of PhP, a large number of H bonds are formed due to the interaction between the PhP "arm" and the DNA bases as compared to MB. As the temperature increases from 25^0C to 70^0C, there is small variation of the number of hydrogen bonds (Fig. S15). The role played by this interaction mode is more prominent in the case of PhP than compared to MB thus making the minor groove binding the only stable binding mode (Fig. S16). This is completely the opposite of $[Os(bpy)_2dppz]^{2+}$ and MB probes where intercalation modes are the most stable.

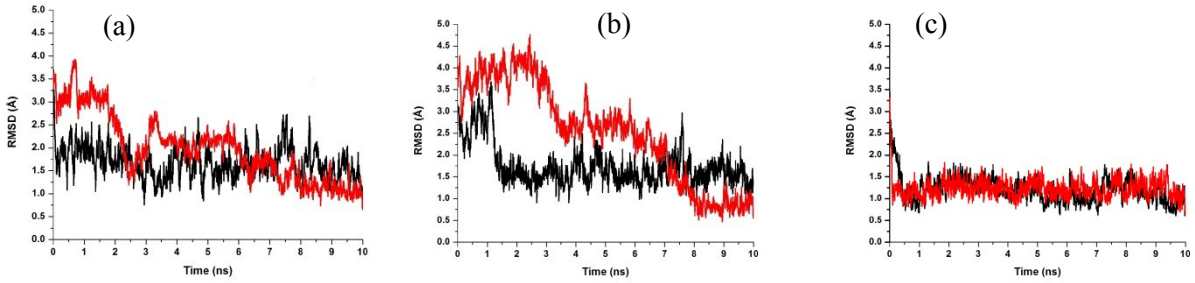

Fig. S14 Plot of the RMSD obtained for the PhP / 1BNA complex for the three binding modes (a) Symmetrical intercalation at 25^0C, Avg RMSD=1.67(0.3)Å (black) and 70^0C, Avg RMSD=2.00(0.7)Å (red), (b) perpendicular intercalation at 25^0C, Avg RMSD=1.74(0.5)Å (black) and 70^0C, Avg RMSD=2.53(1.2)Å (red), and (c) minor groove binding at 25^0C, Avg RMSD=1.21 (0.3)Å (black) and 70^0C Avg RMSD=1.23 (0.2)Å (red).

a

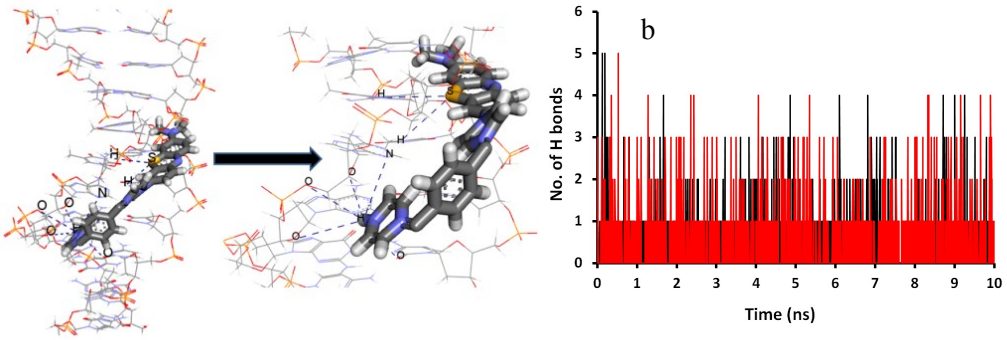

Fig. S15 (a) Snapshot showing the formation of H bonds between 1BNA and PhP. (b) Total number of H bonds formed at T = 25^0C are 756 (black) and at 70^0C are 797 (red) along the 10 ns trajectory.

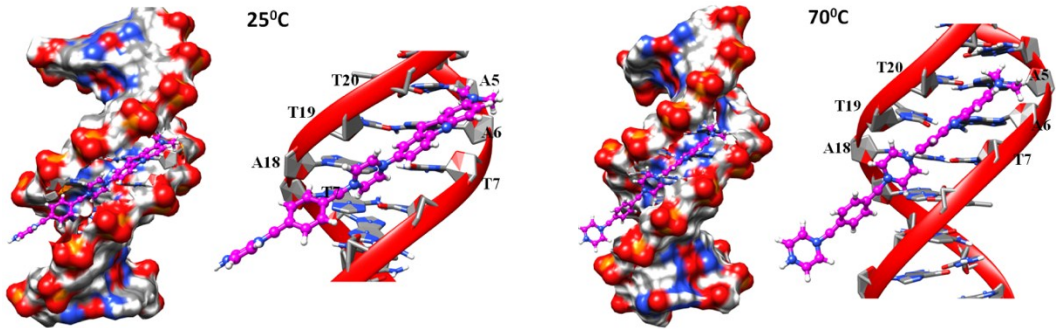

Fig. S16 PhP most stable binding mode: Minor groove binding at T = 25^{0}C and 70^{0}C.

4. Inhibitory effects of the redox probes in electrochemical qPCR

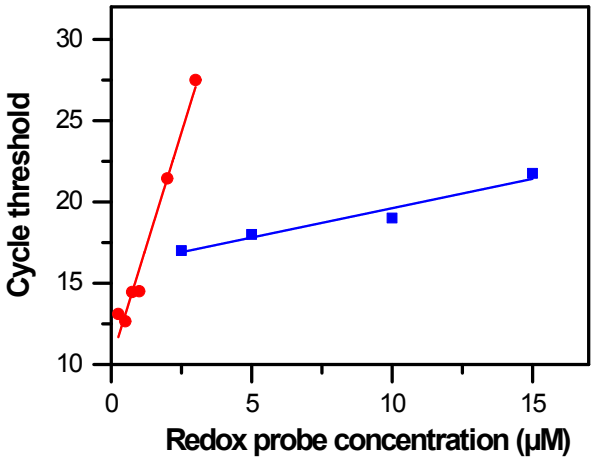

Fig. S17 Comparison of the probe concentration inhibitory effect of (red circles) $[Os(bpy)_2dppz]^{2+}$ and (blue squares) PhP on the C_T value determined for the real-time electrochemical PCR amplification of 10^7 copies of litmus 28i vector.

5. Electrochemical-based qPCR kinetic plots and melting curve analysis using $[Os(bpy)_2dppz]^{2+}$ as an intercalating redox probe

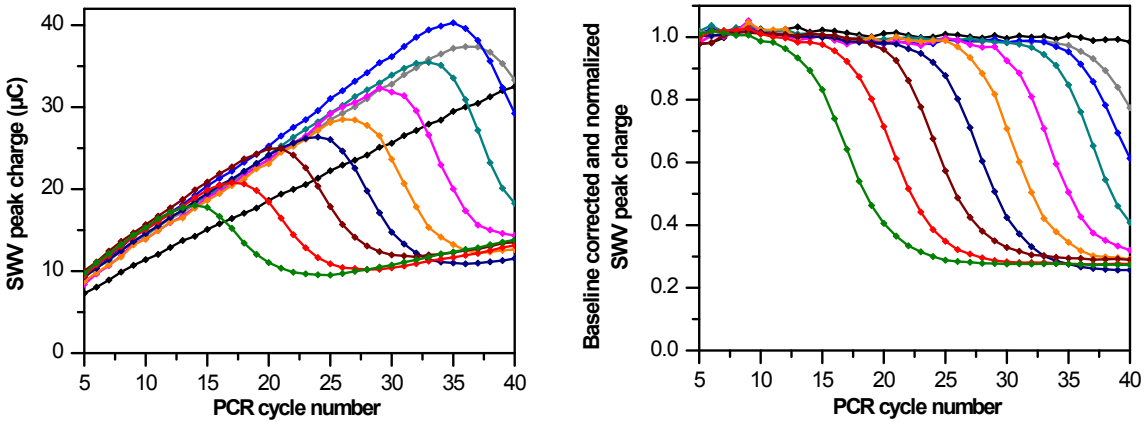

Fig. S18 Left**:** raw evolution of the $[Os(bpy)_2dppz]^{2+}$ SWV peak charge during the electrochemical qPCR amplification of (green) 10^8, (red) 10^7, (brown) 10^6, (dark blue) 10^5, (orange) 10^4, (pink) 10^3, (cyan) 10^2, (blue) 10 and (grey) 0 copies of litmus 28i vector per electrochemical well (for clarity only one kinetic plot per concentration is shown). The black curve is a negative control with no dNTP and no target. The $[Os(bpy)_2dppz]^{2+}$ concentration was 0.5 µM. Right**:** same as in left but after baseline correction and normalization of the kinetic plots.

6. Fluorescence-based qPCR kinetic plots and melting curve analysis

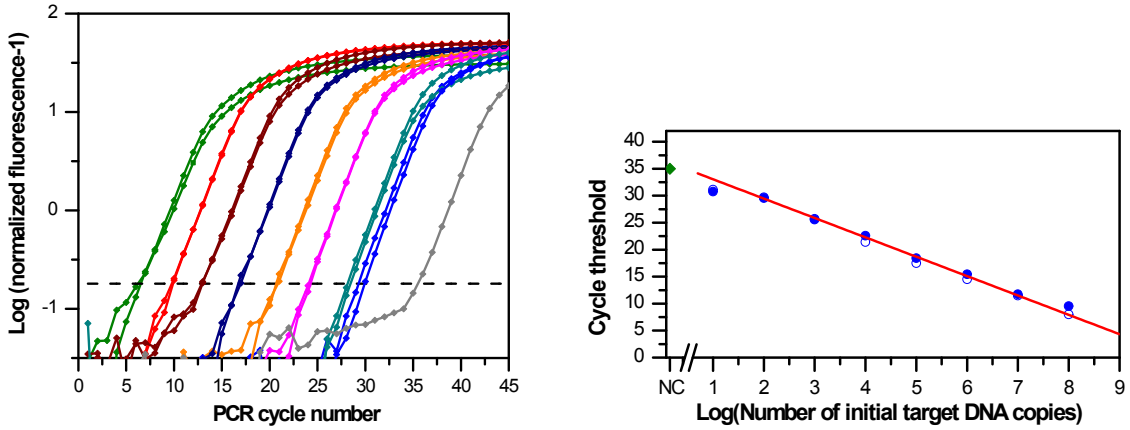

Fig. S19 Left: Semi-logarithmic representation of the baseline corrected amplification curves obtained by fluorescence-based qPCR for a 10-fold serial dilution of standard litmus 28i vector DNA concentrations: (green) 10^8, (red) 10^7, (brown) 10^6, (dark blue) 10^5, (orange) 10^4, (pink) 10^3, (cyan) 10^2, (blue) 10 and (grey) 0 copies of litmus 28i vector per microwell (duplicated measurements except for the 0 copy). The horizontal dashed line is the fluorescence threshold defined as 4-fold the fluorescence baseline noise. Right: Fluorescent-based qPCR calibration plot giving the cycle threshold as a function of the initial target DNA copies per well. The red line is the linear regression fit to the experimental data (ε = 1.90 and R^2 = 0.994). The open diamond corresponds to the negative control (NC, no target DNA).

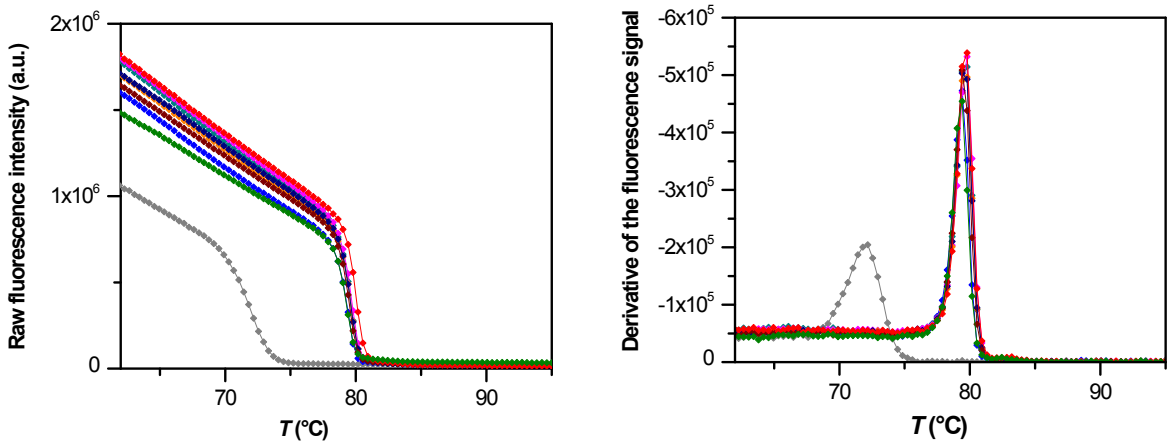

Fig. S20 Melting curve analysis performed immediately after the fluorescence-based qPCR whose results are shown in Fig. S19. Left: raw melting curves resulting from the plot of the fluorescence as a function of the linear ramp of temperature applied to the samples (ramp of 1°C/min ranging from 60°C to 95°C). The colour code is the same than in Fig. S19: (green) 10^8, (red) 10^7, (brown) 10^6, (dark blue) 10^5, (orange) 10^4, (pink) 10^3, (cyan) 10^2, (blue) 10 and (grey) 0 copies of litmus 28i vector per well. Right: first order derivative of melting curves shown on the left graph. All first order derivative melting curves of positive samples (ranging from 10^8 copies to 10 copy) give a maximum peak at an average melting temperature of 80.0 ± 0.5°C, characteristic of right amplified amplicon, while for the 0 copy a maximum peak localised at a melting temperature of ~72°C suggests the presence of short ds-DNA sequence, characteristic of non-specific amplified primer-dimers.

7. References

S1 A. Sharma, S. Delile, M. Jabri, C. Adamo, C. Fave, D. Marchal and A. Perrier, *Phys. Chem. Chem. Phys.*, 2016, **18**, 30029-30039.

S2 J. J. Nogueira and L. González, *Biochemistry*, 2014, **53**, 2391-2412.